Ultrasonics - Sonochemistry 51 (2019) 49–57

Contents lists available at ScienceDirect

Ultrasonics - Sonochemistry

journal homepage: www.elsevier.com/locate/ultson

Effect of different electrolytes and deposition time on the supercapacitor properties of nanoflake-like $Co(OH)_2$ electrodes

N.C. Maile[a], S.K. Shinde[b], R.R. Koli[a], A.V. Fulari[c], D.Y. Kim[b,*], V.J. Fulari[a,*]

[a] Holography and Materials Research Laboratory, Department of Physics, Shivaji University, Kolhapur 416004, M.S., India
[b] Department of Biological and Environmental Science, College of Life Science and Biotechnology, Dongguk University-Ilsan, Biomedical Campus, Goyang-si, Gyeonggi-do 10326, South Korea
[c] Department of Physics, Osmania University, Hyderabad, India

ARTICLE INFO

Keywords:
Electrochemical synthesis
$Co(OH)_2$ thin films
XRD
Nanomaterials
Supercapacitor

ABSTRACT

The effect of ultrasonic treatment and deposition time on nanoflake-like $Co(OH)_2$ thin films were prepared using the potentiostatic mode of electrodeposition method on stainless steel substrates by a nitrate reduction reaction. After ultrasonic treatment, we used stainless steel substrates for deposition of the nanoflakes like $Co(OH)_2$ thin films. The effect of deposition times and electrolytes on different physico-chemical properties of $Co(OH)_2$ was investigated in detail, such as X-ray diffraction (XRD), field emission scanning electron microscopy (FE-SEM), energy dispersive X-ray spectroscopy (EDS), and electrochemical testing. After ultrasonic treatment $Co(OH)_2$ thin films had devolvement of the uniform and interconnected formation of nanoflakes nanostructures. Supercapacitor performance of the $Co(OH)_2$ electrodes suggest that, specific capacitance are depends on the surface morphology, and $Co(OH)_2$ electrodes after ultrasonic treatment exhibited higher performance than without ultrasonication. The maximum specific capacitance of the 30 min. deposited $Co(OH)_2$ nanoflakes exceeded 276 Fg^{-1} in 0.5M KOH electrolyte at 5 mVs^{-1} scan rate.

1. Introduction

Supercapacitors are promising energy-storage devices because of their high-power density and their capability to quickly charge and discharge, which are characteristics desirable for devices used in hybrid vehicles, backup energy systems, and portable electronics [1,2]. Supercapacitors store energy in the form of a double layer or in the form of redox reactions involving a change in the oxidation state during the charging and discharging process [3]. For both mechanisms, functional electrode materials are crucial for the conversion and storage of energy, and they are an essential component of supercapacitors. Among different methods of fabricating functional electrode materials, electrochemical deposition is a simple, binder-free, low-cost method compared with evaporation, sputtering, chemical vapor deposition (CVD), etc.

Homogeneous surface morphologies are of the interesting the formation of different functional coatings for the electrochemical testing. Morphology could be observed, controlled, and studied in electrodeposition by optimizing parameters such as deposition time. Previous studies have investigated the effect of deposition time on surface morphology for metal oxides such as MnO_2 [4], TiO_2 [5], Cu_2O [6,7], Fe_2O_3 [8], and WO_3 [9], hydroxides (Ni–Co)$(OH)_2$ [10], conducting polymers such as polypyrrole [11] and carbon nanotubes [12], etc. These studies have identified the crucial deposition time-dependent properties of these materials. For supercapacitors, transition metal oxides and hydroxides are considered to be the most promising electrode materials. The high-cost RuO is not commercially available even though it has a high specific capacitance [13]. On the other hand, Co$(OH)_2$ is considered to be a promising electrode material due to its layered structure with large interlayer spacing [14]. The electrodeposition method of $Co(OH)_2$ on nickel foam has been demonstrated by Kong et. al. [15]; they found that $Co(OH)_2$ was too thin to form stable and effective structures with a short deposition time, whereas the pores were covered by nanostructured flakes with a longer deposition time, resulting in a significant decrease in the specific capacitance value. Cost-effective stainless steel has been used for the deposition of $Co(OH)_2$ thin films. The cathodic potentiostatic electrodeposition of Co$(OH)_2$ on a stainless steel substrate was reported by Gupta et. al. [16]; they found that the specific capacitance value was not affected by mass loading from 0.1 to 0.8 mg/cm^2. There have been no reports on the specific capacitance values for higher mass loading and higher deposition time. The significance of deposition time in electrodeposition method and the effect of the different electrolytes on the specific

* Corresponding authors.
E-mail addresses: sbpkim@dongguk.edu (D.Y. Kim), vijayfulari@gmail.com (V.J. Fulari).

https://doi.org/10.1016/j.ultsonch.2018.09.003
Received 26 September 2017; Received in revised form 30 August 2018; Accepted 2 September 2018
Available online 07 September 2018
1350-4177/

capacitance of $Co(OH)_2$ thin films should be investigated collectively.

This study was carried out to systematically to investigate the effect of time on pattern formation using the potentiostatic mode of electrodeposition method and to evaluate the effect of different electrolytes. Analytical grade cobalt nitrate dissolved in double-distilled water was used for deposition. A constant cathodic potential of 1.0 V was applied for deposition times of 10, 20, 30, and 40 min. In addition, to optimize the electrolyte for supercapacitors, analytical grade potassium hydroxide (KOH), sodium hydroxide (NaOH), and sodium sulfate (Na_2SO_4) were used. The study mainly focused on optimization; a 0.5M concentration was selected. High specific capacitance values could be possible with higher concentrations of KOH, NaOH, and Na_2SO_4 electrolytes [17].

2. Experimental details

2.1. Chemicals

All chemicals used for synthesis were of analytical grade; thus, no further purification was required. Cobalt (II) nitrate hexahydrate [$Co(NO_3)_2{\cdot}6H_2O$], KOH, NaOH, and Na_2SO_4 electrolytes were obtained from Thomas Baker India Pvt. Ltd.(Mumbai, India).

2.2. Synthesis of $Co(OH)_2$ thin films

$Co(OH)_2$ thin films were deposited on stainless steel substrate (grade 304, 0.03 cm thick) substrate using the potentiostatic mode of electrodeposition method in an electrolyte bath (60 mL) containing 0.1M of $Co(NO_3)_2{\cdot}6H_2O$ at room temperature (300 K). The pH of the solution was ~6. The conventional three-electrode system was used for deposition as shown in Fig. 1. A stainless steel substrate with a dimension of 1 × 5 cm was used as the working electrode, a graphite plate (G) with a dimension of 1.5 × 6 × 0.2 cm was used as the counter electrode, and a saturated calomel electrode (SCE) was used as the reference electrode. The stainless steel substrate and graphite electrode were kept suspended in the electrolyte solution 1 cm apart. Prior to deposition, all the electrodes were washed and cleaned with double distilled water. The stainless steel substrate was polished with zero-grade polish paper. To remove any remaining surface contamination, cleaned substrates were etched in 10% H_2SO_4 for 2 min and rinsed with double-distilled water by ultrasonication [18].

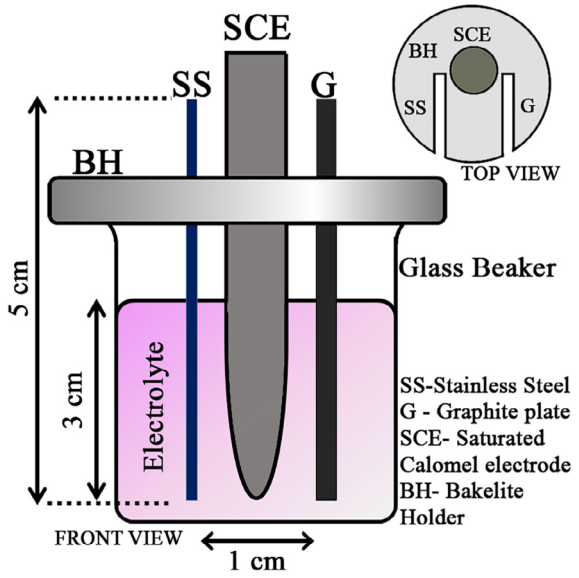

Fig. 1. Schematic diagram showing front view and side view of electrolyte bath setup.

In order to determine the effect of deposition time, a constant potential of −1.0 V [19] was applied to the stainless steel substrate (3 cm^2 dipped) with respect to the SCE for 10, 20, 30, and 40 min. The prepared samples were named as S-10, S-20, S-30, and S-40. The structural, morphological, and electrochemical properties of the deposited $Co(OH)_2$ thin films were characterized. For phase confirmation, X-ray diffraction (XRD; Bruker D2 phaser table-top model) analysis was performed with a copper target (Cu-K_α radiation; K = 1.54 Å) at a diffraction angle (2θ) from 10° to 80°. The surface morphology of the films was observed by field emission scanning electron microscopy (FE-SEM; Mira-3; Tescan Pvt., Brno, Czech Republic.). Electrochemical testing was carried out using cyclic voltammetry (CV), charge–discharge (CD) techniques, and electrochemical impedance spectroscopy (EIS). EIS was performed over a frequency range of 0.01–1 MHz using a CH Instruments electrochemical workstation (Model CHI-660-D).

2.3. Electrode preparation and electrochemical measurement

The deposited $Co(OH)_2$ on stainless steel substrate was directly used for electrochemical testing without any preparation. Electrochemical measurements were carried out using three-electrode cell configurations with $Co(OH)_2$ samples as the working electrode, platinum as the counter electrode, and SCE as the reference electrode with 0.5M KOH electrolyte, 0.5M NaOH electrolyte, or 0.5M Na_2SO_4 electrolyte as the electrolytes. CV measurements of the $Co(OH)_2$ electrode were performed at different scan rates with a potential window of −0.4 to 0.4 V. CD characterization was performed at different current densities with a potential window of −0.4 to 0.4 V.

To see the feasibility of $Co(OH)_2$ electrode, the symmetric device was fabricated by conventional way. The $Co(OH)_2$ electrodes on two stainless steel substrate substrates of 1 cm^2 area each were soaked in polymer–KOH gel. The each soaked electrode after drying pressed one another to form a symmetric device (SS/$Co(OH)_2$/Poly-KOH/$Co(OH)_2$/SS). The CV and CD testing of device was performed for 0.4 V potential window. The stability of device was tested for 1000 cycles.

2.4. Electrochemical parameters

Based on cyclic voltammetry (CV) measurements, the capacitance was calculated using the following formula (for three-electrode configurations) [19,20]:

$$C_{sp}^{CV} = \frac{\oint I(V)dV}{2 \times m \times r \times (V_f - V_i)} F\ g^{-1} \quad (1)$$

Similarly, based on constant current charge–discharge (CD) measurements, the specific capacitance of the material was evaluated using the following formula:

$$C_{sp}^{CD} = \frac{I_{dis} \times \Delta t}{m \times (V_f - V_i)}\ F\ g^{-1} \quad (2)$$

where, C_{sp}^{CV} and C_{sp}^{CD} are the specific capacitance calculated using CV and CD measurements, respectively. 'm' is the mass of one electrode, 'r' is the scan rate, V_f − Vi is the potential window, and $\oint I(V)dV$ is the area under the CV curve. I_{dis} is the discharge current at which the measurement was performed. 'Δt' is the discharge time.

3. Results and discussion

3.1. Ultrasonication procedure for stainless steel substrate

Ultrasonication method of substrate surface is very important before any further process. In simple experiment, the deposition of $Co(OH)_2$ was performed on stainless steel substrates with and without ultrasonication treatment. Fig. S1 in supplementary shows the FESEM images of without and with ultrasonication of stainless steel substrates

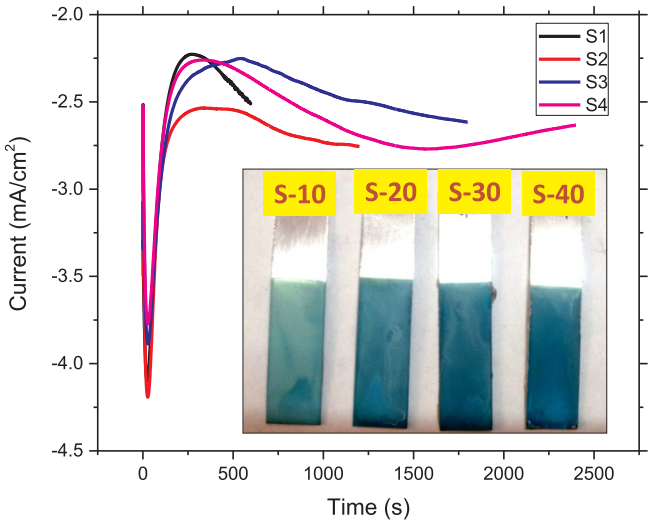

Fig. 2. The potentiostatic deposition curve for S-10, S-20, S-30, S-40 observed for applied potential of −1.0 V/SCE. Inset shows photograph images of thin films.

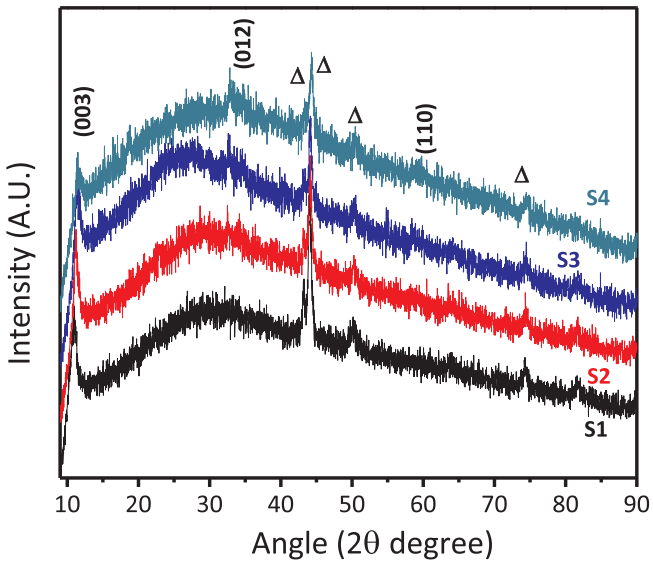

Fig. 3. XRD patterns of $Co(OH)_2$ samples with different deposition time.

at two different magnification. It clearly demonstrated that ultrasonication affected the growth of $Co(OH)_2$ thin films. Uniform growth was seen in ultrasonically cleaned stainless steel substrate. So prior to deposition all substrates were cleaned ultrasonically.

3.2. Reaction and growth mechanism of $Co(OH)_2$ thin films

The potentiostatic deposition curve of the samples S-10, S-20, S-30, and S-40 are shown in Fig. 2. A rapid increase in the cathodic current was observed initially, and it subsequently decreased with time. The initial increase in current may be attributed to the growth of a new phase or an increase in the number of nucleation centers. During deposition growth, the nuclei develop diffusion zones around themselves, which can lead to hemispherical mass transfer followed by linear mass transfer, resulting in the effective planar surface. The subsequent decrease in current corresponds to linear diffusion. The nature of these curves is a typical example of 3D multiple nucleations with diffusion-controlled growth [7,21]. With an applied potential of −1.0 V, both the hydrogen evolution reaction and the reduction of NO^{3-} are possible. Both reactions could lead to an increase in OH^- ion concentration at the stainless steel surface. As shown in the inset of Fig. 2, the OH^- ions could react with Co^{2+} ions from the electrolyte, leading to the formation of a bluish-green colored $Co(OH)_2$ nanomaterial coating on the stainless steel surface. The deposition of $Co(OH)_2$ on the SS surface can be expressed by the following possible reactions [22,23]:

$$NO^{3-} + H_2O + 2e^- \rightarrow NO^{2--} + 2OH^- \quad (1)$$

$$NO^{3-} + 7H_2O + 8e^- \rightarrow NH^{4+} + 10OH^- \quad (2)$$

$$2H_2O + 2e^- \rightarrow H_{2(g)} + 2OH^-_{(aq)} \quad (3)$$

$$Co^{2+} + 2OH^- \rightarrow Co(OH)_2 \quad (4)$$

Because of the rough surface, the thickness of the film was measured in terms of deposited mass using the weight difference method. It was found to be 1.2 mg, 3.7 mg, 4.0 mg, and 3.8 mg on an effective surface area of 3 cm^2 for S-10, S-20, S-30, and S-40 respectively. Initially, as the deposition time was increased, the deposited mass was increased; however, the mass was subsequently decreased over time due to the rapid thickening and flaking of the deposits.

3.3. X-ray diffraction analysis

Fig. 3 shows the XRD pattern of $Co(OH)_2$ thin films synthesized using the electrodeposition method for various deposition times. All samples were polycrystalline in nature with a α-$Co(OH)_2$ phase. All peaks were well matched with the standard JCPDS card 46-0605. The peaks present at 11.01°, 33.03°, and 59.71° corresponded to the (0 0 3), (0 1 2), and (1 1 0) planes, respectively. In addition, some broad peaks had a low intensity, suggesting the formation of nanocrystalline materials [14,25]. A small number of reflection peaks is an indication of poorly ordered samples. The strong low-angle reflection peak at 2θ = 11.01° had a d-spacing of 8.02 Å. This can be attributed to nitrate groups intercalated into the hydrotalcite-like α-$Co(OH)_2$ thin films [26]. Energy dispersive X-ray spectroscopy (EDS) analysis (Fig. 4) of S-30 revealed that it contained Co and O with a ratio of about 1:2 [27]. The C peak observed in EDS results may be associated with the carbon conducting tape on which the sample was mounted during EDS analysis.

3.4. Morphological analysis of $Co(OH)_2$ thin films

Fig. 5 shows the FE-SEM images of the S-10, S-20, S-30, and S-40 samples at two different magnifications. Fig. 5a and b clearly show that at a deposition time of 10 min, the substrate was not uniformly covered with the nanostructured material due to the insufficient growth time of $Co(OH)_2$ thin films after the formation of a smaller number of nucleation centers on the substrate. As the deposition time was increased to 20 min, the number of nucleation centers was increased gradually, leading to the growth of vertically aligned nanoflakes with large spaces between them as shown in Fig. 5c and d. With a further increase in deposition time from 20 to 30 min, the substrate was uniformly covered with interconnected porous nanoflakes as shown in Fig. 5e and f. The interconnected porous nanoflakes had a high surface area, which was better for the intercalation of ions into the electrode surface. A further increase in deposition time from 30 to 40 min led to the agglomeration of interconnected porous nanoflakes due to overgrowth as shown in Fig. 5g and h. A similar observation was reported in another study [28]. The deposition time-related growth mechanism is shown in Scheme 1.

Electrochemical properties largely depend on the surface morphology of thin films. In supercapacitors, the charge storage mechanism is different for electrostatic double-layer capacitors (EDLCs) and pseudocapacitors. In an EDLC, most of the charge is accumulated at the surface of the electrode material; thus, it requires a large surface area. In the case of a pseudocapacitor, the charge is stored via the Faradaic reaction at the interface between the electrolyte and electrode, where the phase of the material changes during the charging and discharging

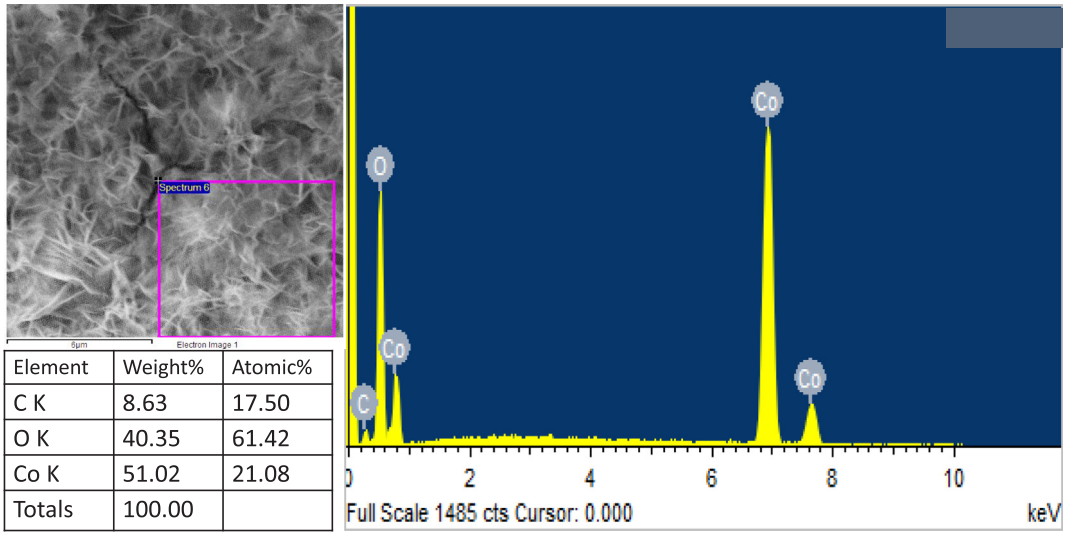

Element	Weight%	Atomic%
C K	8.63	17.50
O K	40.35	61.42
Co K	51.02	21.08
Totals	100.00	

Fig. 4. EDS analysis S-30 $Co(OH)_2$ thin film surface.

process. For a pseudocapacitor, the electrode surface must be highly porous so that the ions in the electrolyte can diffuse and interact with the material [29]. Based on FE-SEM analysis, the S-30 sample was uniformly deposited and had a maximum mass loading; hence, it was used for further electrochemical testing with different electrolytes.

3.5. Electrochemical analysis

3.5.1. Effect of different electrolytes

Electrochemical testing of the S-30 sample was performed in different electrolytes (0.5M Na_2SO_4 electrolyte, 0.5M NaOH electrolyte, and 0.5M KOH electrolyte). Fig. 6a and b show the CV curve and galvanostatic CD curve of the $Co(OH)_2$ electrode (S-30) in different electrolytes. The mirror image of CV and CD curves suggests the evolution of Faradaic reactions at the electrode–electrolyte interface during the charging and discharging process. Fig. 6a and b show that KOH is the best electrolyte for further electrochemical analyses. Supporting Figs. S2 and S3 show the CV curves of the S-30 sample in NaOH and Na_2SO_4 electrolytes with different scan rates (5–100 mV/s). Fig. 6c and d show the plot of the calculated specific capacitance as a function of different scan rates and current densities for different electrolytes. The diffusion time for ions in the active material was decreased with an increase in scan rate and current density values, as shown in Fig. 6c. The specific capacitance was decreased with respect to scan rate for the sample in KOH, NaOH, and Na_2SO_4. In Na_2SO_4, the surface intercalation and de-intercalation of Na^+ resulted in redox reactions at the electrode-electrolyte interface due to the adsorption of Na^+ from the electrolyte to the electrode surface. In KOH and NaOH, the redox reaction involved OH^-.The possible electrochemical reactions corresponding to Faradaic reactions can be expressed as follows [30,31]:

$$Co(OH)_2 + OH^- \leftrightarrow CoOOH + H_2O + e^- \quad (5)$$

$$CoOOH + OH^- \leftrightarrow CoO_2 + H_2O + e^- \quad (6)$$

The specific capacitance from the cyclic voltammetry (CV) plot was calculated using Eq. (1) for 0.5M Na_2SO_4, 0.5M NaOH, and 0.5M KOH electrolytes at 5 mV s^{-1}, which was determined to be 0.75 Fg^{-1}, 189.23 Fg^{-1}, and 276.00 Fg^{-1}, respectively. The specific capacitance from the current charge–discharge (CD) plots was calculated using Eq. (2) for 0.5M Na_2SO_4, 0.5M NaOH, and 0.5M KOH electrolytes at 1 $mAcm^{-2}$, which was determined to be 0.04 Fg^{-1}, 180.47 Fg^{-1}, and 272.95 Fg^{-1}, respectively. The maximum specific capacitance was 276.00 Fg^{-1} for the sample in the KOH electrolyte at 5 mV s^{-1}; this may be attributed to the higher current response in solutions containing OH^- compared with other electrolytes. A similar result was observed in Fig. 6d, which shows the current density with respect to the specific capacitance. Furthermore, similar results were reported for $Ni(OH)_2$ in a previous study [32].

EIS is an important technique for supercapacitor applications as it can be used to clarify electrode kinetics and the mechanistic aspects involved. EIS measurements were performed at the open circuit potential (OCP) over a frequency range of 0.1–1 MHz with an applied potential of 5 mV. Fig. 7a shows typical Nyquist plots for $Co(OH)_2$ in the 0.5M Na_2SO_4, 0.5M NaOH, and 0.5M KOH electrolytes. Fig. 7b shows the equivalent circuit for the EIS and magnified EIS data of $Co(OH)_2$ in 0.5M KOH electrolyte. At high frequencies, the intercept of the real impedance (Z') represents a combined resistance of the electrolyte, intrinsic resistance of substrate, and contact resistance at the active material-current collector interface known as the equivalent series resistance or solution resistance (R_S). A sharp increase in Z_{im} at lower frequencies may be attributed to the capacitive behavior of the material; however, a semi-circle at higher frequencies would imply that the charge transfer resistance (R_{ct}) at the electrode/electrolyte interface is mainly associated with Faradaic reactions and double-layer capacitance (C_{dl}) at the surface [33]. The slope of the 45° portion of the curve is called Warburg resistance (Z_w) and is the result of the frequency dependence of ion diffusion from the electrolyte to the electrode surface. The limit capacitance (Cl) is associated with voltage-dependent Faradaic charge transfer. The fitted circuit element parameters of EIS are presented in Table 1. The R_s of the S-30 sample in KOH was 2.63 Ω/cm^2, which was lower than that of the S-30 sample in Na_2SO_4 (4.23 Ω/cm^2) and NaOH (5.40 Ω/cm^2), indicating a lower contact resistance. The lower R_{ct} (1.93 Ω/cm^2) of the sample in KOH indicated the improved transfer and faster transfer rate of ions in the KOH electrolyte compared with the Na_2SO_4 (32.62 Ω/cm^2) and NaOH (5.77 Ω/cm^2) electrolytes. The R_{ct} and R_s values demonstrated that KOH is the best electrolyte compared with others. Fig. 7c and d show the frequency-dependent impedance (Z) values and frequency-dependent phase values (Bode plots), respectively, for 0.5M Na_2SO_4, 0.5M NaOH, and 0.5M KOH electrolytes.

3.5.2. Effect of different deposition times

$Co(OH)_2$ electrodes was found to have a maximum specific capacitance value in 0.5M KOH electrolyte. Therefore, the electrochemical analysis of S-10, S-20, S-30, and S-40 electrodes was performed in 0.5M KOH electrolyte. The cyclic voltammetry plot at a scan rate of 10 mVs^{-1} in 0.5M KOH electrolyte with a potential window of −0.4 to +0.4 V/SCE is shown in Fig. 8a. All samples had prominent oxidation

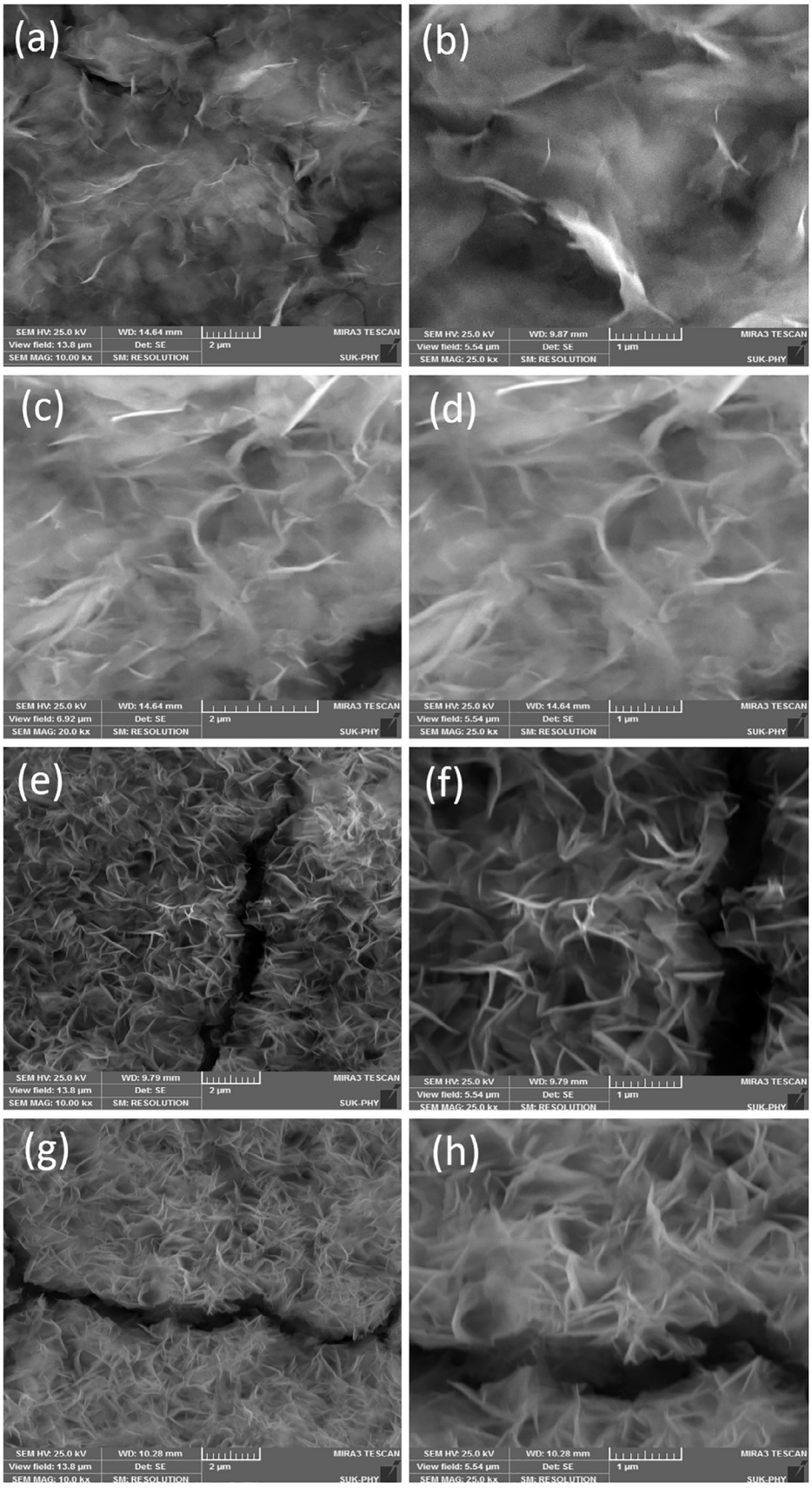

Fig. 5. The FESEM images of $Co(OH)_2$ thin films deposited at 10 min. (a, b), 20 min (c, d), 30 min. (e, f), and 40 min. (g, h) with different magnification, respectively.

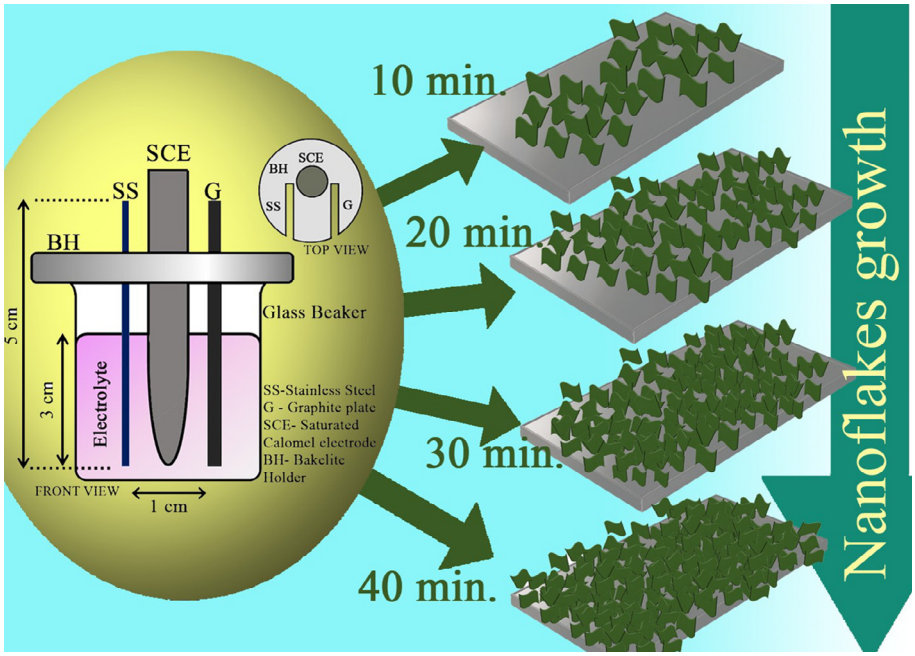

Scheme 1. The growth formation of $Co(OH)_2$ thin films with different deposition time.

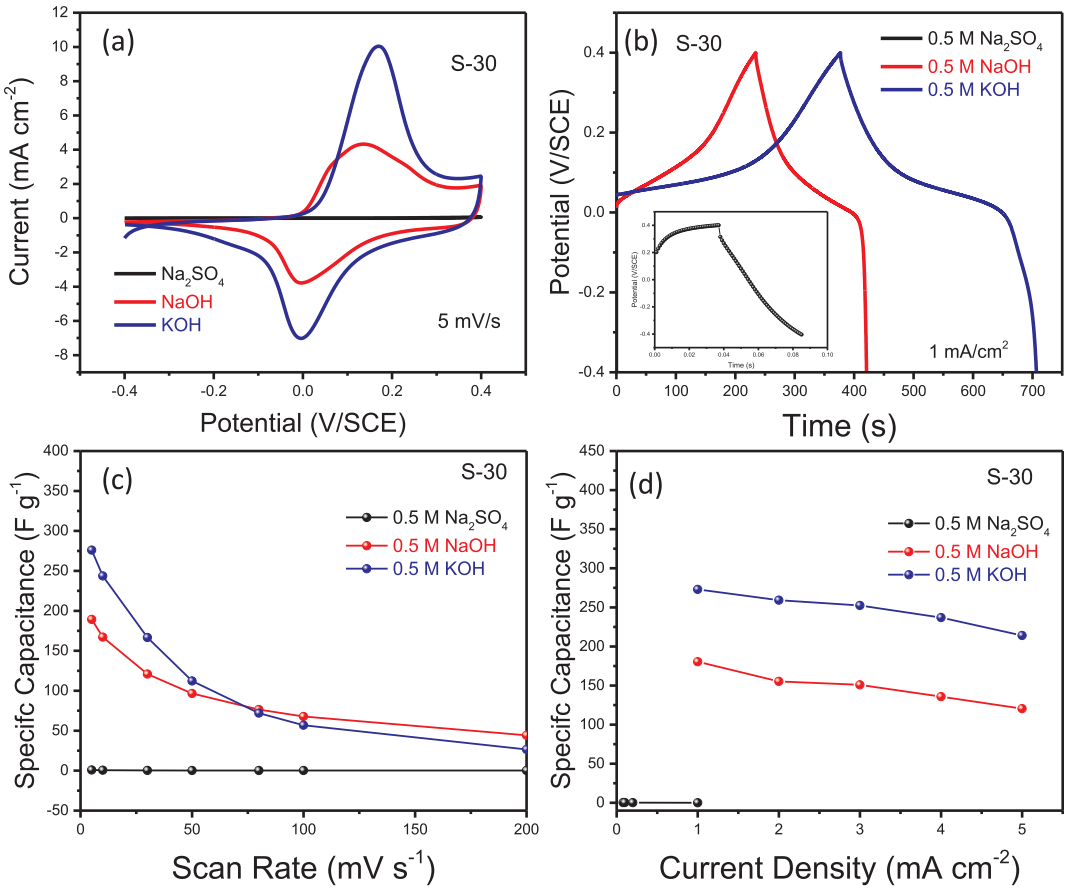

Fig. 6. (a) The CV curve of S-30 samples in 0.5M Na_2SO_4, 0.5M NaOH and 0.5M KOH, (b) CD curve of S-30 film in 0.5M Na_2SO_4, 0.5M NaOH and 0.5M KOH, (c) The plot of specific capacitance values for S-30 film from cyclic voltammetry curve in 0.5M Na_2SO_4, 0.5M NaOH and 0.5M KOH, (d) The plot of specific capacitance values for S-30 film from charge discharge curve in 0.5M Na_2SO_4, 0.5M NaOH and 0.5M KOH.

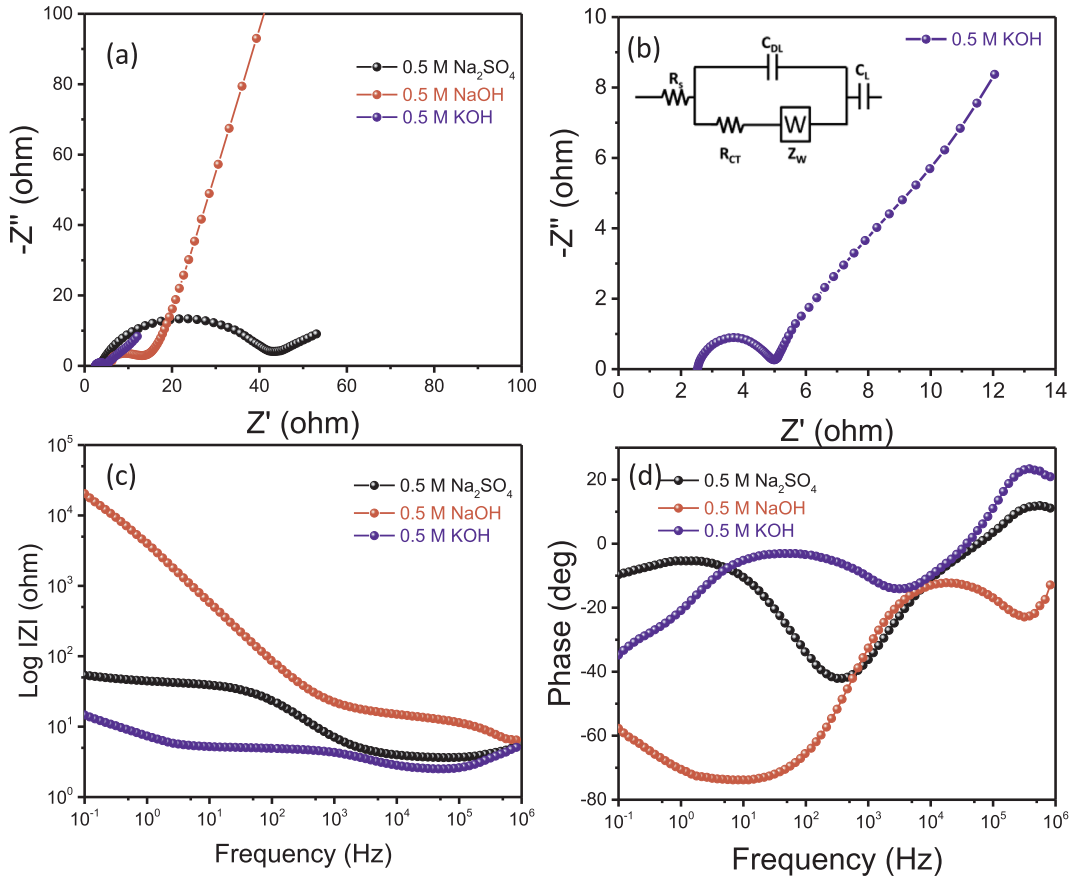

Fig. 7. Nyquist (a) plot of S-30 for 0.5M Na_2SO_4, 0.5M NaOH and 0.5M KOH electrolyte; (b) EIS equivalent circuit and magnified Nyquist plot for 0.5M KOH; (c) Frequency dependent Impedance Bode plots for 0.5M Na_2SO_4, 0.5M NaOH and 0.5M KOH (d) Frequency dependent Phase Bode plots for 0.5M Na_2SO_4, 0.5M NaOH and 0.5M KOH.

Table 1
Calculated values of R_S, C_{DL}, R_{CT}, Z_W and C_L through fitting of the experimental EIS based upon the proposed equivalent circuit in Fig. 8.

Parameter	Na_2SO_4	NaOH	KOH
$R_S(\Omega)$	4.23	5.40	2.63
$C_{DL}(F)$	3.97×10^{-5}	9.45×10^{-8}	3.28×10^{-5}
$R_{CT}(\Omega)$	32.62	5.77	1.93
$Z_W(\Omega)$	5.68×10^{-2}	8.52×10^{-4}	1.2×10^{-1}
$C_L(F)$	1.14×10^{20}	4.08×10^{-5}	1.23

and reduction peaks, indicating the storage of charges in the form of redox reactions [30]. In comparison with other electrodes, S-30 was observed to have maximum current response. The charge-discharge plots at a current density of 1 $mAcm^{-2}$ in 0.5M KOH electrolyte is shown in Fig. 8b. The calculated values of the specific capacitance at 1 $mAcm^{-2}$ current density were 190.46 Fg^{-1}, 258.89 Fg^{-1}, 272.92 Fg^{-1}, and 203.12 Fg^{-1} for the $Co(OH)_2$ electrode deposited with deposition times of 10, 20, 30, and 40 min, respectively. Initially, the specific capacitance of the electrode was increased with the load of $Co(OH)_2$ materials and reached the maximum when the load was 4.0 mg at 30 min; this may be attributed to an increase in the load of Co $(OH)_2$ electrodes on steel substrate, which could provide more active sites. However, with a further increase in time, the load was decreased from 4.0 mg to 3.8 mg, and the specific capacitance of the electrode was reduced from 272.92 to 203.12 Fg^{-1}. These results may be explained by considering the effects of load increase. With an increase in the load of $Co(OH)_2$, the active material for the Faradaic charge transfer reaction could increase. Consistently, FE-SEM microimages revealed that the number of nanoflakes was increased up to 30 min. At 40 min, the mass of the material was decreased due to the overloading of the $Co(OH)_2$ material, which could cause cracks in the films. The agglomeration of nanoflakes could decrease the diffusion of electrolyte ions [34,35].

Fig. 8c shows the cyclic voltammetry plots of the $Co(OH)_2$ electrode synthesized using the electrodeposition method for 30 min (S-30) at various scan rates (5–200 mV/s) in 0.5M KOH electrolyte, and the inset shows the corresponding CD plot. As the scan rate of CV was increased, oxidation and reduction potential values were increased, which may be attributed to the limited diffusion of ions into the active material of the $Co(OH)_2$ electrodes. The diffusion time of electrolyte ions was decreased as the scan rate was increased. The $Co(OH)_2$ thin film had a maximum specific capacitance value of 276 $F\,g^{-1}$ in 0.5M KOH electrolyte at 5 mVs^{-1}. The previously reported specific capacitance values is shown in Table 2 [16,24,36–40]. Fig. 8d shows the plot of the calculated specific capacitance at different current densities for the S-10, S-20, S-30, and S-40 samples.

To evaluate the feasibility of synthesized $Co(OH)_2$ as supercapacitor electrode material. The symmetric device was fabricated using polymer-KOH gel electrolyte. Fig. S4a shows cyclic voltammetry of symmetric device at different scan rates (5–100 $mV\,s^{-1}$) which is rectangular in shape which is associated with common phenomena of metal oxides hybrid electrode materials of pseudo rate constant of charging and discharging over voltammetry cycle [41]. Fig. S4b shows CD of symmetric device at different current densities (0.5–0.9 $\mu A\,cm^{-2}$), which is symmetric in shape. The plot of calculated specific capacitance values from CV and CD curve is shown in Fig. S4(c, d). The maximum specific capacitance calculated was found to be 0.18 Fg^{-1} for 0.5 μA. The stability of device evaluated for 1000 cycles with capacity retention of 81.9% which is shown in Fig S4e. The CD curves at constant current value of 1 μA for 1st and 1000th cycle is

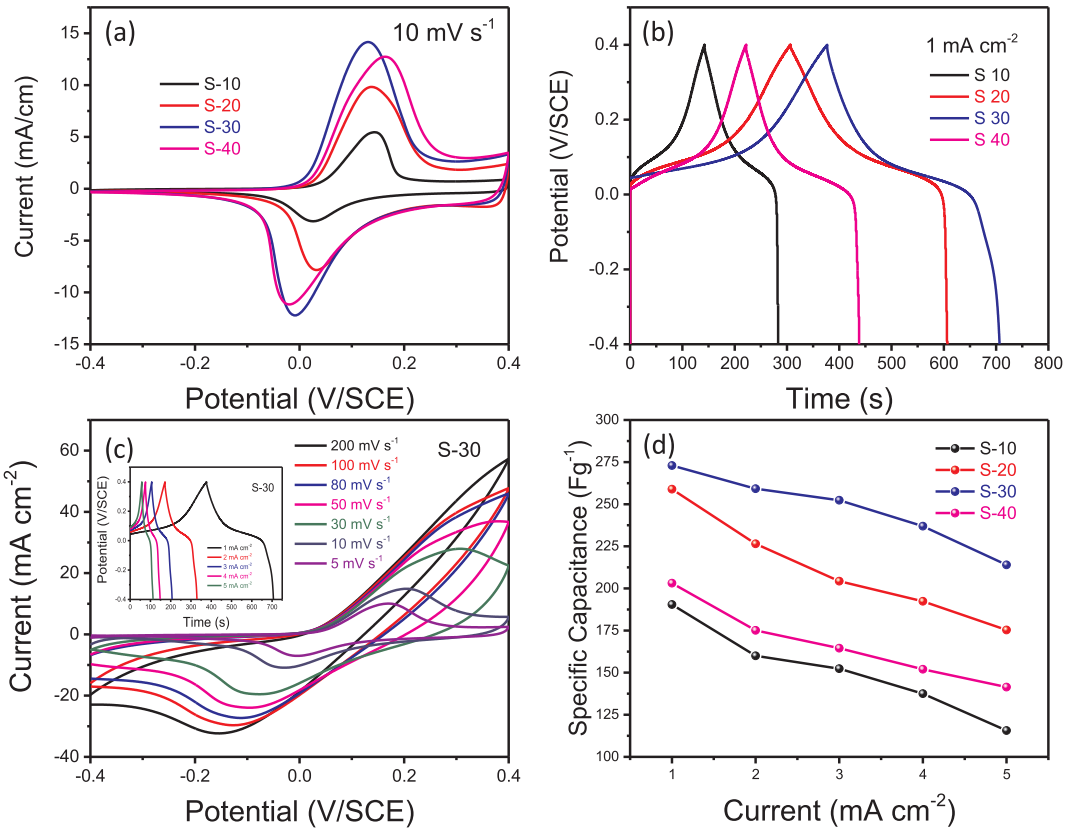

Fig. 8. (a) The cyclic voltammetry curve of S-10, S-20, S-30 and S-40 electrodes in 0.5M KOH at 5 mV/s, (b) The plot of specific capacitance values of S-10, S-20, S-30 and S-40 electrodes in 0.5M KOH at 5 mV/s, (c) The CV plot of S-30 electrode in 0.5M KOH electrolyte for different scan rates, (d) Specific capacitance values of S-30 electrode at different scan rates (5–200 mV/s).

Table 2
Comparative study of our supercapacitor electrode material performance with various electrode materials.

Electrode material	Synthesis method	Nanostructure of electrodes	Electrolyte	Specific Capacitance	Ref. no.
$Co(OH)_2$ on S.S.	Potentiostatic	Compact nanosheet	1M KOH	881 F g^{-1} at 1 A g^{-1}	36
$Co(OH)_2$ on Nickel grid	Precipitation	Mesoporous	1M KOH	341 F g^{-1} at 5 mA cm^{-2}	37
$Co(OH)_2$ on Nickel grid	Precipitation	loose whisker	2M KOH	325 F g^{-1} at 20 mA cm^{-2}	38
$Co(OH)_2$	Potentiostatic	Ordered mesoporous	1M KOH	993 F g^{-1} at 1 A g^{-1}	39
$Co(OH)_2$	Hydrothermal	Nnanocones	2M KOH	562 F g^{-1} at 2 A g^{-1}	40
$Co(OH)_2$ on Nickel grid	Chemical precipitation	Nanoflakes	2M KOH	735 F g^{-1} at 5 mA cm^{-2}	41
$Co(OH)_2$ on S.S.	Potentiostatic	Dense layered	1M KOH	651 F g^{-1} at 2 A g^{-1}	24
Co(OH)2 on SS	*Potentiostatic*	*Interconnected nanoflakes*	*0.5 M KOH*	272.9 *Fg*$^{-1}$ *at* 1 mA cm^{-2}	*Present work*

shown in Fig. S4f which shows decrease in discharge time. The calculated energy density and power density for device is depicted in Regone plot of Fig. S5.

4. Conclusion

Ultrasonic treatment produces the $Co(OH)_2$ thin films with different morphologies, which were successfully synthesized by a simple and low-cost electrodeposition method. The effect of ultrasonic treatment and deposition time on structural, morphological, and electrochemical properties of $Co(NO_3)_2$ films has been investigated. XRD patterns confirmed the formation of $Co(OH)_2$ material with a polycrystalline in nature with a α-$Co(OH)_2$ phase. FE-SEM results shown the development different nanostructures of $Co(OH)_2$ thin films deposited at different deposition times. Supercapacitor performance revealed that the KOH electrolyte contributed to maximum specific capacitance. The maximum specific capacitance of the $Co(OH)_2$ thin films shows 276 Fg^{-1} at a scan rate of 5 mVs^{-1} in 0.5 KOH electrolyte. The 30 min. deposited Co $(OH)_2$ electrode shows the higher surface area, more capable, and better supercapacitor performance.

Acknowledgement

The authors are grateful to UGC for financial assistance through the UGC Major Research Project (F.No.43-532/2014 (SR) MRP-MAJOR-PHYS-2013-35168 dated 07/10/2015).

Appendix A. Supplementary data

Supplementary data associated with this article can be found, in the online version, at https://doi.org/10.1016/j.ultsonch.2018.09.003.

References

[1] D.P. Dubal, Y.P. Wu, R. Holze, Supercapacitors: from the Leyden jar to electric busses, ChemTexts 2 (2016) 13, https://doi.org/10.1007/s40828-016-0032-6.
[2] S.K. Shinde, D.P. Dubal, G.S. Ghodake, D.Y. Kim, V.J. Fulari, Nanoflower-like CuO/$Cu(OH)_2$ hybrid thin films: synthesis and electrochemical supercapacitive properties, J. Electroanal. Chem. 732 (2014) 80–85, https://doi.org/10.1016/j.jelechem.

2014.09.004.
[3] S. Zhang, N. Pan, Supercapacitors performance evaluation, Adv. Energy Mater. 5 (2015) 1401401, https://doi.org/10.1002/aenm.201401401.
[4] C.A. Castro Ruiz, D. Bélanger, D. Rochefort, Electrochemical and spectro-electrochemical evidence of redox transitions involving protons in thin MnO_2 electrodes in protic ionic liquids, J. Phys. Chem. C 117 (2013) 20397–20405, https://doi.org/10.1021/jp405047g.
[5] L.A. Pereira, A.B. Couto, D.A. de, L. Almeida, N.G. Ferreira, The influence of TiO_2 amount on the photoactivity response for the novel TiO_2/BDD/carbon fiber ternary composite, Diam. Relat. Mater. 75 (2017) 18–24, https://doi.org/10.1016/j.diamond.2016.12.018.
[6] N. Binti Mohamad Arifin, F. Mohamad, C. Hui Ling, N. Binti Zinal, A.S. Binti Mohd Hanif, N.H. Muhd Nor, M. Izaki, Growth mechanism of copper oxide fabricaticated by potentiostatic electrodeposition method, Mater. Sci. Forum. 890 (2017) 303–307, https://doi.org/10.4028/www.scientific.net/MSF.890.303.
[7] M.M. Moharam, E.M. Elsayed, J.C. Nino, R.M. Abou-Shahba, M.M. Rashad, Potentiostatic deposition of Cu_2O films as p-type transparent conductors at room temperature, Thin Solid Films 616 (2016) 760–766, https://doi.org/10.1016/j.tsf.2016.10.005.
[8] M.Z. Shaiful Azni, H.K. Tan, P.L. Low, N.K. Devaraj, B.H. Ong, T.Y. Tou, Electrodeposited iron(III) oxide (α-Fe_2O_3) thermoelectric thin films, Key Eng. Mater. 701 (2016) 23–27, https://doi.org/10.4028/www.scientific.net/KEM.701.23.
[9] J. Lee, W. Choi, H. Shin, Preparation of electrolytic tungsten oxide thin films as the anode in rechargeable lithium battery, Korean J. Mater. Res. 23 (2013) 680–686, https://doi.org/10.3740/MRSK.2013.23.12.680.
[10] X. Gong, J.P. Cheng, F. Liu, L. Zhang, X. Zhang, Nickel-Cobalt hydroxide microspheres electrodepositioned on nickel cobaltite nanowires grown on Ni foam for high-performance pseudocapacitors, J. Power Sources. 267 (2014) 610–616, https://doi.org/10.1016/j.jpowsour.2014.05.120.
[11] J.V. Thombare, V.J. Fulari, M.C. Rath, S.H. Han, Optical absorption study of electrochemically synthesized polypyrrole(Ppy) thin films, 2012 Int. Conf. Opt. Eng., IEEE, 2012, pp. 1–4, , https://doi.org/10.1109/ICOE.2012.6409569.
[12] H. Fayazfar, A. Dolati, M. Ghorbani, Electrochemical characterization of electrodeposited carbon nanotubes, Thin Solid Films 519 (2011) 6230–6235, https://doi.org/10.1016/j.tsf.2011.03.123.
[13] D.P. Dubal, N.R. Chodankar, R. Holze, D.-H. Kim, P. Gomez-Romero, Ultrathin mesoporous $RuCo_2O_4$ nanoflakes: an advanced electrode for high-performance asymmetric supercapacitors, ChemSusChem 10 (2017) 1771–1782, https://doi.org/10.1002/cssc.201700001.
[14] S. Bae, J.-H. Cha, J.H. Lee, D.-Y. Jung, Nanostructured cobalt hydroxide thin films as high performance pseudocapacitor electrodes by graphene oxide wrapping, Dalt. Trans. 44 (2015) 16119–16126, https://doi.org/10.1039/c5dt02161h.
[15] L. Bin Kong, M.C. Liu, J.W. Lang, M. Liu, Y.C. Luo, L. Kang, Porous cobalt hydroxide film electrodeposited on nickel foam with excellent electrochemical capacitive behavior, J. Solid State Electrochem. 15 (2011) 571–577, https://doi.org/10.1007/s10008-010-1125-6.
[16] V. Gupta, T. Kusahara, H. Toyama, S. Gupta, N. Miura, Potentiostatically deposited nanostructured α-$Co(OH)_2$: a high performance electrode material for redox-capacitors, Electrochem. Commun. 9 (2007) 2315–2319, https://doi.org/10.1016/j.elecom.2007.06.041.
[17] Y. Gao, S. Chen, D. Cao, G. Wang, J. Yin, Electrochemical capacitance of Co_3O_4 nanowire arrays supported on nickel foam, J. Power Sources 195 (2010) 1757–1760, https://doi.org/10.1016/j.jpowsour.2009.09.048.
[18] S.K. Shinde, G.S. Ghodake, D.P. Dubal, R.V. Patel, R.G. Saratale, D.-Y. Kim, N.C. Maile, R.R. Koli, H.D. Dhaygude, V.J. Fulari, Electrochemical synthesis: monoclinic Cu_2Se nano-dendrites with high performance for supercapacitors, J. Taiwan Inst. Chem. Eng. 75 (2017) 271–279, https://doi.org/10.1016/j.jtice.2017.01.028.
[19] L.-B. Kong, M.-C. Liu, J.-W. Lang, M. Liu, Y.-C. Luo, L. Kang, Porous cobalt hydroxide film electrodeposited on nickel foam with excellent electrochemical capacitive behavior, J. Solid State Electrochem. 15 (2011) 571–577, https://doi.org/10.1007/s10008-010-1125-6.
[20] S. Sahoo, S. Ratha, C.S. Rout, Spinel $NiCo_2O_4$ nanorods for supercapacitor applications, Am. J. Eng. Appl. Sci. 8 (2015) 371–379, https://doi.org/10.3844/ajeassp.2015.371.379.
[21] S. Ratha, S.R. Marri, N.A. Lanzillo, S. Moshkalev, S.K. Nayak, J.N. Behera, C.S. Rout, Supercapacitors based on patronite–reduced graphene oxide hybrids: experimental and theoretical insights, J. Mater. Chem. A 3 (2015) 18874–18881, https://doi.org/10.1039/C5TA03221K.
[22] F.R. Bento, L.H. Mascaro, Analysis of the initial stages of electrocrystallization of Fe, Co and Fe-Co alloys in chloride solutions, J. Braz. Chem. Soc. 13 (2002) 502–509, https://doi.org/10.1590/S0103-50532002000400015.
[23] J.R.S. Brownson, C. Lévy-Clément, Electrodeposition of α- and β-cobalt hydroxide thin films via dilute nitrate solution reduction, Phys. Status Solidi. 245 (2008) 1785–1791, https://doi.org/10.1002/pssb.200879534.
[24] T. Zhao, H. Jiang, J. Ma, Surfactant-assisted electrochemical deposition of α-cobalt hydroxide for supercapacitors, J. Power Sources 196 (2011) 860–864, https://doi.org/10.1016/j.jpowsour.2010.06.042.
[25] A.S. Pillai, R. Rajagopalan, A. Amruthalakshmi, J. Joseph, A. Ajay, I. Shakir, S.V. Nair, A. Balakrishnan, Mesoscopic architectures of $Co(OH)_2$ spheres with an extended array of microporous threads as pseudocapacitor electrode materials, Colloids Surf. A Physicochem. Eng. Asp. 470 (2015) 280–289, https://doi.org/10.1016/j.colsurfa.2015.01.068.
[26] I. Kelpšaite, J. Baltrušaitis, E. Valatka, Electrochemical deposition of porous cobalt oxide films on AISI 304 type steel, Medziagotyra 17 (2011) 236–243, https://doi.org/10.5755/j01.ms.17.3.586.
[27] B.R. Jia, M.L. Qin, S.M. Li, Z.L. Zhang, H.F. Lu, P.Q. Chen, H.Y. Wu, X. Lu, L. Zhang, X.H. Qu, Synthesis of mesoporous single crystal $Co(OH)_2$ nanoplate and its topotactic conversion to dual-pore mesoporous single crystal Co_3O_4, ACS Appl. Mater. Interfaces. 8 (2016) 15582–15590, https://doi.org/10.1021/acsami.6b02768.
[28] S.K. Shinde, G.S. Ghodake, D.P. Dubal, G.M. Lohar, D.S. Lee, V.J. Fulari, Structural, optical, and photo-electrochemical properties of marygold-like $CdSe_{0.6}Te_{0.4}$ synthesized by electrochemical route, Ceram. Int. 40 (2014) 11519–11524, https://doi.org/10.1016/j.ceramint.2014.03.063.
[29] G.Z. Chen, Supercapacitor and supercapattery as emerging electrochemical energy stores, Int. Mater. Rev. (2016) 1–30, https://doi.org/10.1080/09506608.2016.1240914.
[30] A.D. Jagadale, V.S. Jamadade, S.N. Pusawale, C.D. Lokhande, Effect of scan rate on the morphology of potentiodynamically deposited β-$Co(OH)_2$ and corresponding supercapacitive performance, Electrochim. Acta 78 (2012) 92–97, https://doi.org/10.1016/j.electacta.2012.05.137.
[31] T. Nguyen, M. Boudard, L. Rapenne, O. Chaix-Pluchery, M.J. Carmezim, M.F. Montemor, Structural evolution, magnetic properties and electrochemical response of $MnCo_2O_4$ nanosheet films, RSC Adv. 5 (2015) 27844–27852, https://doi.org/10.1039/C5RA03047A.
[32] Z. Ren, J. Li, Y. Ren, S. Wang, Y. Qiu, J. Yu, Large-scale synthesis of hybrid metal oxides through metal redox mechanism for high-performance pseudocapacitors, Sci. Rep. 6 (2016) 20021, https://doi.org/10.1038/srep20021.
[33] Z. Gao, W. Yang, Y. Yan, J. Wang, J. Ma, X. Zhang, B. Xing, L. Liu, Synthesis and exfoliation of layered α-$Co(OH)_2$ nanosheets and their electrochemical performance for supercapacitors, Eur. J. Inorg. Chem. (2013) 4832–4838, https://doi.org/10.1002/ejic.201300525.
[34] C. Gong, M. Huang, J. Zhang, M. Lai, L. Fan, J. Lin, J. Wu, Facile synthesis of $Ni_{0.85}Se$ on Ni foam for high-performance asymmetric capacitors, RSC Adv. 5 (2015) 81474–81481, https://doi.org/10.1039/C5RA09476C.
[35] C. Xu, J. Liao, R. Wang, P. Zou, R. Wang, F. Kang, C. Yang, MoO_3 @Ni nanowire array hierarchical anode for high capacity and superior longevity all-metal-oxide asymmetric supercapacitors, RSC Adv. 6 (2016) 110112–110119, https://doi.org/10.1039/C6RA20579H.
[36] C. Yuan, X. Zhang, B. Gao, J. Li, Synthesis and electrochemical capacitance of mesoporous $Co(OH)_2$, Mater. Chem. Phys. 101 (2007) 148–152, https://doi.org/10.1016/j.matchemphys.2006.03.013.
[37] C. Yuan, L. Hou, L. Shen, D. Li, F. Zhang, C. Fan, J. Li, X. Zhang, A novel method to synthesize whisker-like $Co(OH)_2$ and its electrochemical properties as an electrochemical capacitor electrode, Electrochim. Acta. 56 (2010) 115–121, https://doi.org/10.1016/j.electacta.2010.09.037.
[38] T. Xue, X. Wang, J.-M. Lee, Dual-template synthesis of $Co(OH)_2$ with mesoporous nanowire structure and its application in supercapacitor, J. Power Sources 201 (2012) 382–386, https://doi.org/10.1016/j.jpowsour.2011.10.138.
[39] F. Cao, G.X. Pan, P.S. Tang, H.F. Chen, Hydrothermal-synthesized $Co(OH)_2$ nanocone arrays for supercapacitor application, J. Power Sources 216 (2012) 395–399, https://doi.org/10.1016/j.jpowsour.2012.05.073.
[40] L.-B. Kong, J.-W. Lang, M. Liu, Y.-C. Luo, L. Kang, Facile approach to prepare loose-packed cobalt hydroxide nano-flakes materials for electrochemical capacitors, J. Power Sources 194 (2009) 1194–1201, https://doi.org/10.1016/j.jpowsour.2009.06.016.
[41] N. Parveen, S.A. Ansari, S.G. Ansari, H. Fouad, N.M. Abd El-Salam, M.H. Cho, Solid-state symmetrical supercapacitor based on hierarchical flower-like nickel sulfide with shape-controlled morphological evolution, Electrochim. Acta 268 (2018) 82–93, https://doi.org/10.1016/j.electacta.2018.01.100.